



**Partial gap in two-leg ladders with Rashba effect and its experimental signatures in Si(553)-Au**Piotr Chudzinski *School of Mathematics and Physics, Queen's University of Belfast and Institute of Fundamental Technological Research, Polish Academy of Sciences, Pawinskiego 5B, 02-105 Warsaw, Poland*Julian Aulbach, Jörg Schäfer, and Ralph Claessen *Physikalisches Institut and Würzburg-Dresden Cluster of Excellence ct.qmat, Universität Würzburg, D-97074 Würzburg, Germany*Lenart Dudy *TEMPO Beamline, Synchrotron SOLEIL, L'Orme des Merisiers Saint-Aubin, B.P.48, 91192 Gif-sur-Yvette, France and Physikalisches Institut and Würzburg-Dresden Cluster of Excellence ct.qmat, Universität Würzburg, D-97074 Würzburg, Germany*

(Received 29 April 2021; revised 22 September 2021; accepted 11 October 2021; published 8 November 2021)

We study the effects of Rashba splitting on two-leg ladders with weakly screened Coulomb interactions. Past research has shown that in this class of systems the two backscattering channels with the largest amplitude favor ordering of canonically conjugated collective fields which effectively renders the system gapless. Here we show that the band-dependent Rashba spin-orbit interaction breaks this symmetry of scattering channels, leading to a new fixed point with yet unexplored instabilities. Exotic properties can be found, for instance, the mixing of the magnetism with the charge-density wave. We then investigate the physical consequences of this partial spectral gap opening. We find a striking difference in signatures of order observed in single-particle (spectral-function) and two-body (susceptibilities) experimental probes. We conclude this paper by comparing theoretical and experimental results obtained on the Au-Si(553) platform. In STM measurements, we identify the lowest-lying soliton excitation as a hallmark of the gapped sine-Gordon model in an apparently metallic system. This implies the presence of partial spectral gaps opening. Furthermore, by ARPES measurements we confirm the expected temperature dependence of the outer bands backfolding. These two findings constitute the experimental evidence of the many-body physics proposed here.

DOI: [10.1103/PhysRevB.104.205407](https://doi.org/10.1103/PhysRevB.104.205407)**I. INTRODUCTION**

This work is dedicated to the theoretical description of artificial nanoscale-sized systems which can be generated by the self-organization of atoms absorbed onto appropriate substrate surfaces. The behavior of the electrons in such low-dimensional systems can deviate significantly from the single-particle picture [1]. Novel phases, with nontrivial (i.e., non-*s*-wave) local symmetry of the order parameter are available. They are sometimes called “exotic” phases due to the quite complex structure of their gap in momentum space. These exotic phases are then offering new functionalities, e.g., electric field controlled spin filters for spintronics devices [2] or magnetic field control of an orbital index in the emergent field of valleytronics [3,4]. The interest in such phases has become even stronger since the discovery of topological states, because of Majorana fermions (or parafermions) state existing at the interface between topologically distinct orders.

Theoretical considerations can give us an understanding of how to obtain such exotic phases, using the following procedure: For low-dimensional systems, we start from a highly nontrivial strongly correlated state—the Tomonaga-Luttinger liquid (TLL) of collective bosonic modes [5]. Then, we add (possibly nonlinear) perturbations that lock optimal (energy minimizing) onto the bosonic modes and, hence, open

spectral gaps. With a multitude of bosonic fields in a model, we have many distinct locking combinations and so many distinct order parameters can be defined. Hence, exotic phases may appear. In this context, two-leg ladders are of special interest because they are the first step from simplest one mode one-dimensional systems (1D) to richer two-dimensional systems (2D) and with four modes (eight fields) can host a multitude of exotic phases. These phases are usually driven by two-particle electron-backscattering terms. Hence, Hubbard-type models are used, occasionally with broken symmetries or frustration. Unfortunately, such modeling is not applicable in artificially created platforms on surfaces; the interactions are (at least partially) unscreened and have a long-range (Coulomb-type) character. We know that [6] for these systems, the compressibility of the charge (holon) mode is much smaller than one,<sup>1</sup>  $K_{\rho+} \ll 1$ . Therefore, a TLL description is required. Furthermore, the amplitudes of the backscattering terms are not only small but also perfectly compensated [6]. This causes that any many-body gap, if existent at all, appears only at ultralow temperatures—in the range of  $10^{-4}$  K. We show an example of such compensation in Sec. II B which we describe as a frustration of the scattering channels.

<sup>1</sup>See Eq. (1) for the definitions of symbols.

In contrast to these exotic phases driven by two-particle backscattering terms, the standard Peierls scenario [7] requires single-particle backscattering terms. These are highly relevant in renormalization group (RG) theory and easily open a spectral gap at, or very close to, commensurate fillings. The gap is well described by a mean-field BCS-like theory. Small compressibility and the lattice softness on the surface enhance the propensity for a Peierls mechanism [1]. This is rather unfortunate since these trivial single-particle phenomena are masking potentially nontrivial many-body spectral gaps that bring in the desired exotic phases. It is of particular interest to find a theoretical scenario that allows overcoming this paradigm.

Here, we draw attention to the artificial surface-system Si(553)-Au. In this system, experiments showed several remarkable observations [8–29]. On one hand, clear signatures of density wave formations have been detected—these include bands’ backfolding and real space density patterns. On the other hand, the system is known to be slightly incommensurate and stays metallic down to the lowest measured temperatures/energies. This suggests that, while the standard single-particle physics is not able to develop a gap, there is some other mechanism capable of ordering the system. Curiously enough, the only symmetry-breaking component detectable is the Rashba splitting. Explaining this situation is a challenge for theory that we tackle in this paper.

In the past, a lot of attention was paid to the role of Rashba splitting in 1D systems [30,31]. In particular, an interest was on how various schemes of spin-orbit coupling change the compressibilities and velocities of the gapless TLL modes [32–34], aiming for spintronic applications such as spin filters [35,36]. Interactions were either not present or only included as small perturbation while the spin-orbit terms were much larger [37,38]—up to the point that they were imposing different bosonization schemes [39,40]. Not much effort has been dedicated to the opposite limit, with large relevant interactions and small Rashba-split states, probably because it has been assumed that large interactions will anyway dominate the physics. Hence, the mechanism proposed in this paper has been overlooked. It should also be mentioned that a vast majority of numerical studies, where any regime of parameters can be in principle accessed, has been dedicated to Hubbard-type models with short-range interactions [41]. Our mechanism prefers the situation of partially screened long-range interactions, much harder to implement numerically. Overall, what has been omitted so far is the role of the Rashba effect in setting the amplitudes of the nonlinear terms in the Hamiltonian—those terms that are responsible for the spectral gaps. Our investigation here shows that the presence of Rashba split introduces an unconventional type of incommensurability that breaks the symmetry. The compensation mechanism between scattering channels leads to a relatively large gap opening. This is a mechanism of a phase transition that relies on the cooperation between one-body and two-body terms.

### A. Si(553)-Au: Basic information

An important aspect of the theoretical research has always been the search for realistic systems. A remarkable part of our study is that we have identified the Si(553)-Au as the platform

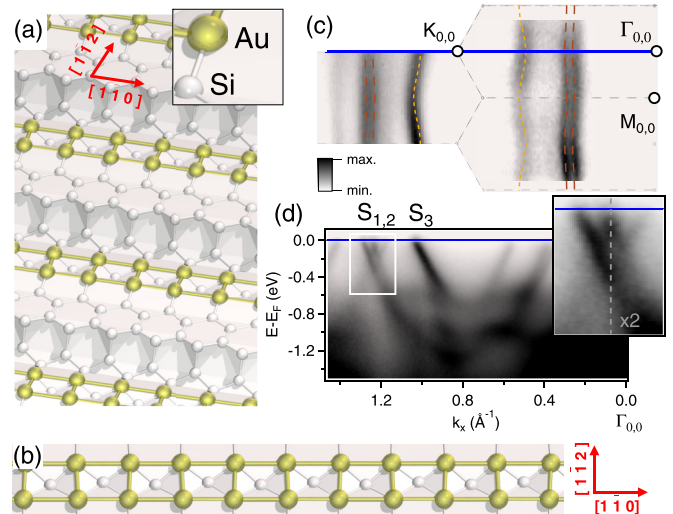


FIG. 1. (a),(b) Structural model of Si(553)-Au enhancing the Au-two-leg ladder. (c) Quasi-1D Fermi surface with the  $1 \times 1$  surface Brillouin zone. (d) Energy vs momentum cut showing the dispersion and the Rashba-split band S1/S2 and band S3, all of them originating from the two-leg ladder structure.  $k_x$  is along the  $[1 = 10]$  direction, along the blue line  $\Gamma_{0,0}$ - $K_{0,0}$  in (c).

where our theory can be immediately tested. Si(553)-Au is a surface system where the vicinal Si(553) surface is evaporated with gold [8,9]. It hosts two electronic quasi-one-dimensional (1D) subsystems; one is situated near the double-stranded conducting Au chain and the other the  $1/3$ -hole-filled Si-step edges. Both show distinct different periodicities at low  $T$ ,  $\times 2$  for the Au-chain and  $\times 3$  for the Si-step-edge. The  $\times 3$  is only visible at low temperatures, see, e.g., Ref. [42]. A structural model for this surface system was subsequently refined by experiment [10,11] and density functional theory [12,13] (DFT) constraint by multiple experimental observations with efforts still ongoing [27]. In Figs. 1(a) and 1(b), we highlight the Au chain within the structural model of Ref. [12].

### B. Si(553)-Au: Experimental indications of collective physics

Since its first creation, Si(533)-Au was discussed as a quasi-1D system [14]. The band structure of Si(553)-Au is dominated by two quasi-one-dimensional bands (S1/2 and S3). A tight-binding fit to the corresponding wiggled 1D Fermi surface confirmed the strong one-dimensional character [14] and hopping ratios  $t_{\parallel}/t_{\perp}$  from 10 to  $>40$ . Our ARPES data (see the Appendix for experimental details) in Fig. 1 reconfirms this; here the hopping ratios are  $t_{\parallel}/t_{\perp} = t_{\parallel}/t_{\perp} \approx 10$  for S3 and  $t_{\parallel}/t_{\perp} = t_{\parallel}/t_{\perp} \approx 46(39)$  for S1 (S2).

The Au-derived bands S1 and S2 have [14–16] a filling of about  $1/2$ ; our measurements, see Fig. 1, show 0.56 for S1 and 0.52 for S2. The occupation of band S3 is mostly near  $1/3$  but varies much stronger due to its higher sensitivity, e.g., to dopants or defects [17]. All metallic bands show zone folding at the  $\times 2$  Brillouin zone (BZ) at low  $T$  [16,18]. It is intriguing to trace this folding to a Peierls mechanism. However, a simple Peierls mechanism cannot be the correct explanation: The filling is not *exactly* commensurate [8] and the Au chains are (at least down to 8 meV) metallic [19],

despite older reports [16] from ARPES.<sup>2</sup> Also the surface conductivity indicates metallic behavior at low  $T$ 's, where the  $\times 2$  zone folding is present [20]. One could think that  $\times 2$  folding is due to distorted Au dimers as an inherent structural feature. This might be the case for modified Si(553)-Au surfaces, i.e., by hydrogenation [43] or surplus Au [17], where the strong electron doping may render the dimerization gap more important. However, for the pristine (undoped) Si(553)-Au in the following, we show later on that the relative intensity of the  $\times 2$  folding changes with temperature. Overall, there is a Peierls-like  $\times 2$  backfolding and no clear sign of a gap at low  $T$ .

A weak coupling scenario, where DFT bands are simply perturbed by a small nesting term, cannot explain the ordering. Also, substantial backfolding observed at high temperatures cannot be explained within simple single-particle mean-field theory. The surface conductivity shows power laws, typical for quasi-1D metals [20]. Moreover, recent EELS data clearly shows the presence of quasi-1D metal [21,22] in the spectrum of charge excitations. The data has been fit well by a quasi-1D underscreened Coulomb metal with a velocity distinct from the single-particle Fermi velocity. The study shows intraladder velocity to be smaller than the Fermi velocity  $v_{\rho+} < V_F$ , in agreement with numerical studies of systems close to commensurability, and so one does not expect a typical spin-charge separation but rather enveloping of spinon's dispersion (with velocity  $\bar{V}_F$ , where  $\bar{V}_F$  is an average of Fermi velocities in both bands) by the nonlinear holon's. Furthermore, the holon gap opening by pinning, detected by a finite frequency of the "anisotropic plasmon" peak, is expected in this framework. However, this consistency comes at a price: It is well established, since the seminal work of Haldane [5], that, for *interacting* carriers confined in low-dimensional systems, the single-particle description, the Fermi liquid, breaks down. The low-energy states are not in a one-to-one correspondence with the single-particle states and the single particle reference point has to be substituted with a collective TLL reference point.

Although the physics of Si(553)-Au has been extensively studied using DFT, it has never been investigated by the many-body methods of bosonization and subsequent RG analysis; we aim to fill this gap in the course of developing the theory of our mechanism of partial gap opening. The relation between the full many-body theory and a DFT mean-field approach needs to be clarified here. While DFT is able to provide us with a reasonable density distribution of carriers in the ground state, especially when the problem is determined by Coulomb interactions, distributing these among tentative Kohn-Sham states is never simple. Crucially, the entire correlations physics, missing in the single-particle description, will be built on top of these Kohn-Sham states. That is: One needs to distribute electrons among some single particle states, then *add* electron-electron interactions between these and hope that the resulting action is close to the previously diagonalized form. When the TLL emerges, it requires summing up an infinite series of terms. In this respect, we point out that

<sup>2</sup>In fact, gap determinations by ARPES measurements are hindered very much by the strong photovoltage of the Au-Si interface which make them very complicated—almost impossible.

DFT simulations [12,23] themselves suggest that magnetic phenomena are necessary to explain the behavior of the system. Hence, the two-body exchange processes are unavoidable and relevant. However, these Fock terms are much smaller than the Hartree two-body processes because  $V_{e-e}(q=0) \gg V_{e-e}(q=2k_F)$ . Therefore, if one wants to build the theory correctly, one should first include the Hartree-interaction's terms, and so move to the TLL picture with  $v_{\rho+} \neq V_F$ , and only after that add the Fock terms as perturbations. The Hartree terms manifest as a change in the velocity of the charge holon modes, precisely in the way recently witnessed by EELS experiments [21,22]. Finally, let us point to a very recent study [28] where the importance of correlations on the terrace has been strongly underlined.

### C. Outline of the paper

The paper is organized as follows. We begin (Sec. II A) by introducing the appropriate TLL model that describes the physics of carriers in the two-leg ladder. Then we analyze (Sec. II B) the influence of the Rashba splitting on backscattering processes which enables us to find an effective minimal model that captures the lowest energy physics. We identify (Sec. III A) the modes in which the spectral gap opens and estimate its value. Only half of the bosonic modes (the transversal modes) are gapped, a combination that has not been reported so far. The latter part of the paper is dedicated to properties of such a system. In particular, in Sec. III B we focus on the comparison between the single-particle Green's function and the charge susceptibility which enables one to emphasize the dichotomy of these two probes: The spectral gap opening is very weakly visible in the single-particle Green's function; it is fully visible in the susceptibility. Here we extended the theory to capture the most likely interchain processes (see Fig. 4) that could contribute to an in-gap susceptibility, yet the assertion of negligible two-body correlation does hold. Furthermore, we are able to describe a Peierls-like state with an incommensurable nesting. This state shows an exotic mixing of the magnetism with the CDW amplitude.

Our theoretical predictions are then tested against experiments in Si(553)-Au (Sec. IV) where we find signatures that the sine-Gordon model is indeed realized in our system. Particularly, we show a temperature dependence of the backfolding in ARPES that supports our assumed Peierls-like scenario. By utilizing scanning tunneling microscopy (STM), we show that one important signature of the CDW, namely a zigzag pattern of charge by the transversal mode, is indeed realized. The excitations of the sine-Gordon model are solitons in these Au chains which we detect by our STM measurements. We furthermore explore solitons on the Au chain coupled to solitons on the Si chain. This finding is used to probe the robustness and interactions of the quasi-1D Au-two-leg ladder in relation to the quasi-2D electronic structure of the surface.

## II. MODEL

Our derivation is mostly general about the effect on Rashba splitting on two-leg ladders and our derivation can be adapted to other systems alike, nevertheless we use in the following a



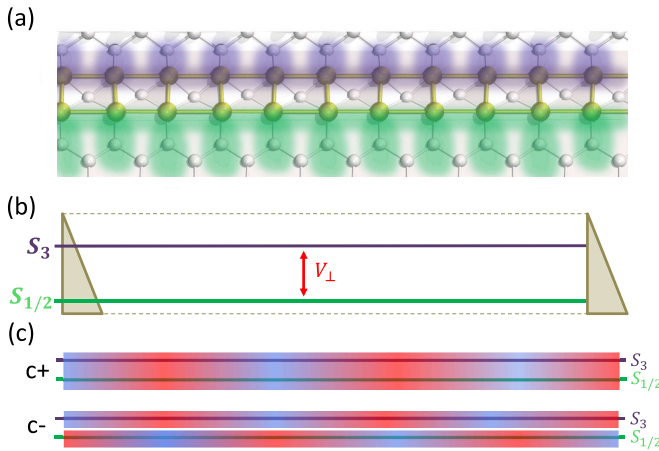


FIG. 2. Real images of the electronic structure under our consideration. Panel (a) shows about the location of the bands S1/2 (purple) and S3 (green) overlaid to the structural model of Ref. [12]. Panel (b) shows the simplification of S1/2 and S3 by two one-dimensional bands with some Coulomb interaction  $V_{\perp}$ . The visualization in panel (c) shows the result of the bozonization after which two charge modes, longitudinal c+ and transversal c- are considered (the two spin modes, longitudinal s+ and transversal s-, are not shown). In the latter course of this paper, we are especially interested in the transversal modes.

nomenclature adapted to the Si553-Au system. In regard to Si553-Au, we focus here on the three metallic bands originating from the Au chain, usually labeled as S1-3. They are well resolved by angular-resolved photoemission spectroscopy (ARPES) at low temperatures, see Figs. 1(c) and 1(d). S1 and S2 are experimentally shown to be a Rashba-split doublet [18,24,25] where the spin-orbit coupling breaks the spin-rotational symmetry on the Au-localized carriers. The split is orders of magnitude smaller than the bandwidth (and presumably also smaller than Coulomb interactions) and so the two-leg ladder description applies. Band S3 belongs to carriers that are more broadly distributed into silicon and its smaller overlap with heavy gold atoms may be the reason why the spin-orbit effects here are much weaker. The single-particle description should provide a good starting point on which the many-body instabilities are constructed provided that the crystal structure is rigid, i.e., not modified substantially by the many-body effects. ARPES confirms this picture.

### A. Two-leg ladder Hamiltonian

When carriers are confined in their motion along one dimension and cannot avoid each other in their motion, the right basis of Hilbert space to describe their physics becomes the basis of collective modes. Re-deriving the theory in such a basis is called bosonization and the anomalous metallic state is called Tomonaga-Luttinger liquid (TLL). A visualization of the modeling is displayed in Fig. 2. Here, Fig. 2(a) shows the localization of the bands S1/2 and S3 on the terrace. Panel (b) shows the simplification of S1/2 and S3 by two one-dimensional bands with some Coulomb-interaction  $V_{\perp}$ . The Hamiltonian of the TLL state is written in terms of fluc-

tuations of these collective modes:

$$H_{\text{TLL}}[v] = \sum_{\nu} \int \frac{dx}{2\pi} \left[ (v_{\nu} K_{\nu}) (\pi \Pi_{\nu})^2 + \left( \frac{v_{\nu}}{K_{\nu}} \right) (\partial_x \phi_{\nu})^2 \right] \quad (1)$$

where  $\nabla \phi_{\nu}(x)$  gives the local density of fluctuation  $v_{\nu}$ ,  $K_{\nu}$  are velocity and TLL parameter ( $\sim$ compressibility) of a given bosonic mode  $\nu$ . Here,  $\nu$  can be  $c\pm, s\pm$ , i.e., we can have collective excitations of each charge and spin type (total and transverse in the two bands). Fermionic operators are written as  $\psi_j \simeq \eta_j \exp(i \sum_{\nu} a_{j,\nu} (\phi_{\nu} + \theta_{\nu}))$  where  $j = S1, S3$  is a band index (defined in the single-particle basis of fermions) and  $a_{i,\nu} = \pm 1$  transforms from band to mode basis. The sum of the responses from S1/2 and S3 gives the total “+” mode, while the difference the transverse “-” mode. Figure 2(c) shows a visualization of the charge modes. The  $\eta_{\nu}$  are the Klein factors which satisfy the required anticommutation relations for fermions. These  $\eta_{\nu}$  do not contain any spatial dependence and commute with the Hamiltonian. They only influence the form of the order operator in bosonic language (by  $\eta_{\nu} \eta_{\nu'}$ ) and the signs of the nonlinear couplings by the  $\Gamma$  coefficient (the eigenvalue of the  $\eta_{\nu} \eta_{\nu'} \eta_{\nu''} \eta_{\nu''}$  operator).  $\Gamma^2 = 1$  and in this paper we choose the convention  $\Gamma = +1$ , as in Ref. [44].

In simplest approximation  $K_c \approx (1 - 2g)$ , where  $g$  is the strength of the Coulomb interaction  $V_{\text{Coul}}(q \rightarrow 0)$ . If the Galilean invariance is obeyed then  $K_{\nu} v_{\nu} = V_F$ , where  $V_F$  is a Fermi velocity  $\sim 2t_b$  (where we take a tight-binding model with the 1D chains arranged along the  $b$  axis) which is  $\sim \Lambda$  (which determines the UV cutoff of our theory). For the spin sector, due to the spin-orbit coupling, the SU(2) spin-rotational invariance is not preserved. This implies that  $K_s$  is not necessarily equal to one. The effect manifests itself as Rashba splitting (at large momentum) and if we assume that it is purely local then its  $q = 0$  component will be of order  $\Delta_R/t_b \sim O(-2)$  which can be neglected in the following. Hence, the TLL theory incorporates all electron-electron interactions of forward scattering type. The interactions are certainly of the Coulomb type, decaying with exchanged momentum  $q$ . This suggest that the backscattering terms are weak. Following past studies on this platform we assume that S1,2 and S3 have a different orbital content. Their single-particle hybridization is weak. However, Coulomb interaction between them  $V_{\perp}$  may still be substantial. We then have an interaction-coupled two-leg ladder. In this case the TLL parameters for the two charge modes are split by  $V_{\perp}$ :  $K_{c\pm} = K_c / \sqrt{1 \pm V_{\perp}}$ , hence both are much smaller than noninteracting value  $K = 1$ .

On the top of Eq. (1), we add the backscattering terms that take the form of cosines in the bosonization formalism. In the two-leg ladder, even if we exclude the Umklapp terms that are impossible away from commensurate filling, we can still have seven backscattering channels of the two-body type:

$$\begin{aligned} H_{\text{int}(1)}^{\text{NL}} = & -g_{1c} \int dr \cos(2\phi_{s+}) \cdot \cos(2\phi_{c-}) \\ & + g_{1a} \int dr \cos(2\phi_{s+}) \cdot \cos(2\phi_{s-}) \\ & - g_{2c} \int dr \cos(2\phi_{c-}) \cdot \cos(2\phi_{s-}) \end{aligned}$$

$$\begin{aligned}
 & + g_{4a} \int dr \cos(2\phi_{s-}) \cdot \cos(2\theta_{s-}) \\
 & + g_1 \int dr \cos(2\phi_{s+}) \cdot \cos(2\phi_{s-}) \\
 & + g_2 \int dr \sin(2\phi_{s-}) \sin(2\phi_{s+}) \\
 & + g_{\parallel c} \int dr \cos(2\phi_{c-}) \cdot \cos(2\theta_{s-}). \quad (2)
 \end{aligned}$$

We use the following notation: Indexes 1 to 4 refer to the standard *g*-ology processes for the left and right moving carriers; letters *a* to *d* correspond to analog processes, when the band's  $j = S1, S3$  index is used instead of the left or right labels. For example, let us take two distinguishable fermions, e.g., with opposite spin, then they can either maintain or change their direction of motion. Then we either have the forward-scattering process “2”:  $L \rightarrow L \ \& \ R \rightarrow L$ , or the backward-scattering process “1”:  $L \rightarrow R \ \& \ R \rightarrow L$ . This is a standard 1D *g*-ology notation. In the presence of a band degree of freedom we can have analogous scattering processes that keep or swap the band index, namely either process “b”  $S1 \rightarrow S1 \ \& \ S3 \rightarrow S3$  or process “a”  $S1 \rightarrow S3 \ \& \ S3 \rightarrow S1$ . In particular there is a possibility of parallel spin cosine process, the band backscattering, as two carriers are distinguishable before/after collision even if their spin is the same. We call it  $g_{\parallel c}$  process. The  $\Gamma$  coefficients determine the signs of the  $g_i$  couplings (this gives minus signs for  $g_{1c}$  and  $g_{2c}$ ).

### B. Effective Hamiltonian

The problem we aim to solve belongs to the two-leg-ladder class. It has been a subject of numerous renormalization group [44,45] and numerical studies [46,47]. In the case of interaction-coupled ladders, most of the cosine terms contain the field  $\phi_{c-}$  (as noticed in Ref. [45] this is contrary to the hybridization coupled ladder, see, e.g., Ref. [44]). Since  $K_{c+} \approx K_{c-} \ll 1$ , all these are potentially strongly relevant. Hence, the renormalization exponent criterion will not suffice to select the dominant ones. The best way forward is to identify backscattering terms which potentially possess the largest amplitude. In the Hubbard-type models, with purely local interactions, all cosine terms have the same amplitude. Moreover, our problem is defined on the surface. Hence, Coulomb interactions are only partially screened. This allows us to profit from the (exchanged) momentum dependence of the electron-electron interactions. In a recent study on two-leg ladders [48], we have shown that, even in the case of partially screened interactions, there still remains a large preference for terms with a smaller momentum exchange. As we see in Fig. 3(a), we can therefore neglect the  $g_{1a}, g_{1c}, g_{1,2}$  terms in Eq. (2) because they involve the *largest momentum transfer* from one side to the opposite side of the Fermi surface. The cosine terms which involve *smaller exchange of momentum* turns out to be those where, upon collision, the left/right movers keep their chirality but change the band. They come in two flavors, as the interacting carriers can have the same (parallel  $\parallel$ ) or the opposite spins. The effective Hamiltonian is

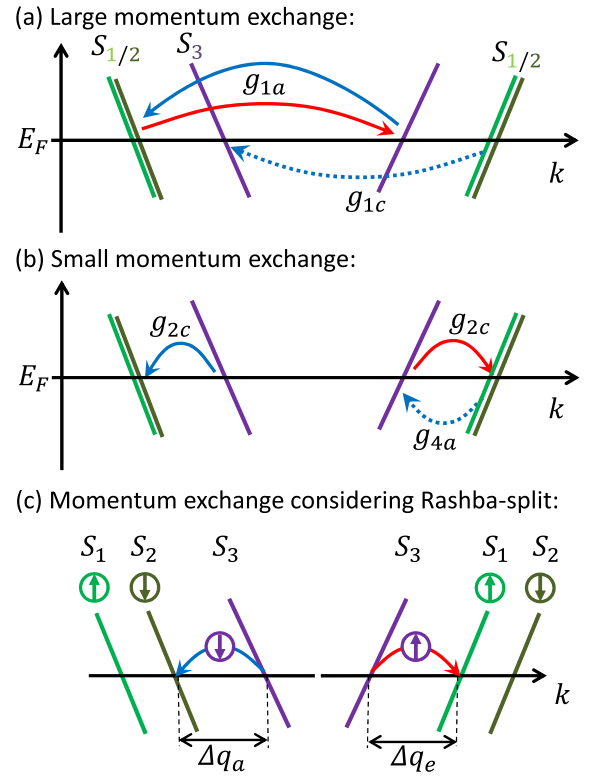


FIG. 3. Visualization of the scattering channels for the linearized bands near  $E_F$ . Panel (a) shows the highest momentum exchange processes  $g_{1a}$  (red+blue arrows), or alternatively  $g_{1c}$  (red + dashed blue). Here red indicates  $L \rightarrow R$  and blue  $R \rightarrow L$  parts of two-body scattering. These are the backscattering processes we neglect. Panel (b) shows smaller momentum exchange processes, e.g.,  $g_{2c}$  (red+blue arrows) or  $g_{4a}$  (red + dashed blue). These we keep because they are an order of magnitude larger. Panel (c) is an inset of (b) showing the effect of the Rashba split. Here bands  $S1$  and  $S2$  are split according to their spin direction. We now see that if the two scattering electrons have opposite spins, the  $g_{2c}$  process (shown), then their momenta,  $\Delta q_a$  and  $\Delta q_e$ , compensate each other precisely. When they have the same spin, the  $g_{\parallel c}$  process (not shown), there is a mismatch of momenta.

then:

$$\begin{aligned}
 H_{\text{eff}} & = g_{\parallel c} \int dr \cos(2\phi_{c-}) \cdot \cos(2\theta_{s-}) \\
 & - g_{2c} \int dr \cos(2\phi_{c-}) \cdot \cos(2\phi_{s-}) \\
 & + g_{4a} \int dr \cos(2\phi_{s-}) \cdot \cos(2\theta_{s-}) \quad (3)
 \end{aligned}$$

so we reduced the number of possible backscattering processes from seven in Eq. (2) (plus four possible Umklapp terms introduced in Appendix B 1 and four possible Peierls terms) down to three that are shown in Fig. 3(b). Please note that graphically  $g_{\parallel c}$  is identical to  $g_{2c}$  with the only difference being that in the first case the two scattering carriers have identical spin.

We emphasize that in the above Hamiltonian the Rashba split is *not* yet taken into account; we assume  $S1, S2$  to be degenerate at this level of the theory. This has the

following consequences. Unfortunately, those two that are possibly the largest among the cosines involve canonically conjugated fields in the transverse spin sector  $\cos 2\phi_{s-}$  and  $\cos 2\theta_{s-}$ . If we now perform the RG procedure, we integrate out the highest energy shells to find how the low energy effective theory is changing; since  $K_{s-} = 1$  then both of these cosines terms are equally relevant and both pull to order the canonically conjugated fields which cannot order simultaneously. The next leading term with smaller momentum exchange  $g_{4a}$  by itself consists out of these two canonically conjugated cosines. We call this behavior in the following a “frustration” of the scattering channels. It is the reason why neither of these is ultimately able to open a gap and in the models with pure Coulomb interactions we need to resort to refermionization and ultimately the many-body theory predicts extremely small spectral gaps of the collective modes.

### III. RASHBA INDUCED EFFECTS

#### A. Gapped modes

We shall now show the way to break this “frustration” of the scattering channels. To this end we introduce the Rashba split of the outer band. Our case now becomes different than the SU(2) invariant situation described above, because the spin-orbit coupling breaks the symmetry between parallel and opposite spin scattering, see Fig. 3(c). As the renormalization group proceeds, we shall reach the scale where due to the S1/2 Rashba split the parallel spin case is much reduced because of the momentum misfit: The right moving spin-up electron transferred from band S3 goes to band S2,  $\Delta q_a = k_{F3} - k_{F2}$ , while the left going spin-up electron has to go from S3 to S1,  $\Delta q_e = k_{F3} - k_{F1}$  (and analogously for spin down and Hermitian conjugate processes). In order to obey the momentum conservation, we need to keep absorbed and emitted on-shell momenta equal  $\Delta q_a = \Delta q_e$  which is clearly not preserved any longer for the parallel spin process. So below the energy  $\approx \Delta_R$ , given by the Rashba split of bands S1/S2, only one of the two selected interband terms survive and the spectral gaps in the  $\phi_{c-}$  and  $\phi_{s-}$  fields immediately open. Crucially, by introducing the Rashba split we do not add any extra term in Eq. (3), but instead we simply change the relative amplitudes of the two-body scattering terms. Ultimately, one of the scattering channels is suppressed down to zero because of the momentum misfit.

Please note that this mechanism is similar to the suppression of Umklapp terms for the slightly incommensurate situation [1] as described in the context of Eq. (B1) (which also takes place in our problem and inhibits opening of large Mott gaps of the  $\phi_{c+}$  mode). However, the novel aspect in here is that the mechanism can select the preferred scattering channel. By employing this analogy, we see that in the RG equation for  $g_{\parallel c}$ , in  $\partial g_{\parallel c}(l)/\partial l$ , we need to multiply the Gell-Mann beta function by  $J_0(l\Delta_R^{-1})$  and this term stops flowing when  $l \approx \Delta_R$  while the flow of the competing term  $g_{2c}$  continues unchecked.

We can further inspect if our mechanism remains valid if we include exchange interactions and higher order terms (stronger interactions). This could possibly enhance the  $g_{4a}$  term and cause a substantial deviation from  $K_{s-} = 1$ . While

the term  $g_{4a}$  by itself is never relevant, it has a nonzero conformal spin which implies that it shall generate two further terms  $G_\phi \int dr \cos(4\phi_{s-})$  and  $G_\theta \int dr \cos(4\theta_{s-})$ . Furthermore, we observe that while for S1/2 the parallel spins  $g_{1d\parallel}^{S12}$  are prohibited by momentum conservation (and same for interband S1/2  $\leftrightarrow$  S3), for S3 these parallel spins are allowed. The spin-flip processes are always allowed. Overall this leads to

$$K_{s-} = 1 - (-2(g_{1d\parallel}^i - g_{1f}^i) + (g_{1d\parallel}^{S12} - g_{1f}^{S12}) + (g_{1d\parallel}^{S3} - g_{1f}^{S3})) < 1.$$

As a result, both of the higher order terms  $\sim G_\phi$  and  $\sim (1 - K_{s-})$  support the ordering on the  $\phi_{s-}$  side.

The sole term  $-g_{2c} \int dr \cos(2\phi_{c-}) \cdot \cos(2\phi_{s-})$  with  $K_{c-} < 1$  shall flow to strong coupling, open a gap, and lock the two bosonic fields in the configuration  $\phi_{c-} = 0$ ,  $\phi_{s-} = 0$  (or  $\phi_{c-} = \pi/2$ ,  $\phi_{s-} = \pi/2$ ). This narrows down the set of possible low-energy orders. Since  $K_{c+} \ll 1$  then, assuming that we are on the density wave side (particle-hole channel), we can look at Umklapp terms which, although with small initial amplitudes, are very relevant and their incommensurability is similar to  $\Delta_{c-}$ . One then observes that  $\phi_{c+} = \pi/2$  is favored for  $\phi_{c-} = 0$ ,  $\phi_{s-} = 0$ . This reduces the set of preferred orderings down to two. With our convention of Klein factors we find that this shall promote the *OAF* – *SDW<sub>z</sub>* with out-of-plane spin-order plus a possible admixture of FCDW supporting diagonal in-plane currents. This ordering will have a periodicity  $2(k_{FS1/2} - k_{FS3})$  which falls close to  $\frac{1}{6}$  BZ. We expect that some parity-symmetry-breaking electronic-liquid displacements may be present at this periodicity. To estimate the value of the gap we note that at low energy BKT flow the  $\Delta_R$  fixes the distance from the separatrix of the flow  $\bar{A}$ . Then the BKT hyperbolic trajectories can be integrated exactly  $g_{2c}[l] = \bar{A}/\text{Sinh}[\bar{A}l^{-1} + \text{ArcTanh}(\bar{A}/y_{\parallel}^{(0)})]$  which by the condition  $g_{2c}[l^*] = 1$  allows us to find the gap  $\Delta_{c-} = \Delta_{s-} = \Delta_R \exp(-l^*)$ . In the specific case of Si(553)-Au the symmetry breaking  $\Delta_R = 50$  meV which leads to  $\Delta_{c-} \approx 7$  meV.<sup>3</sup>

To conclude this section, we were able to show that as along the RG we integrate out the system at longer and longer length scales when we reach the characteristic Rashba-split length it modifies the RG flow and lifts the “frustration” related to pinning of canonically conjugated fields of densities and their momentum. As a result, one of the spin fields and one of the charge fields (both transverse, i.e., density fluctuations perpendicular to the step) open a spectral gap which, for Au-Si(553), is  $2\Delta_{c-} = 14$  meV. Having identified the two bosonic modes with the spectral gaps in their spectrum, we can now investigate physical consequences of this partial gap opening.

#### B. Physical consequences of the partial gap

Two-leg ladders offer a much richer set of instabilities than any simple 1D chain. For instance, when a CDW appears, it can be symmetric or antisymmetric in the bands S1 and S3; it can be also defined on the rungs or on the diagonal bonds.

<sup>3</sup>To obtain this numerical value we also took  $t_b = 1.2$  eV,  $K_{s-} = 1$ ,  $K_{c-} = 1/3$  and  $\bar{A} = \Delta_R/t_b, y_{\parallel}^{(0)} = 1 - (K_{s-} + K_{c-})/2$ .

Since the transverse mode opens the spectral gap and the key emergent physics takes place there, we focus on transverse susceptibility being the best hallmark for these modes. In our case, we have an interaction coupled ladder but also the two bands S1 and S3 (“chains”) which are separated in real space. They occupy distinct areas of each step, therefore the transverse phenomena may be observed as difference of response in the direction perpendicular to the step. Hence, apart from a standard, symmetric CDW where the entire density oscillates in phase (coupled to the  $\phi_{c+}$  mode), we shall also have a zigzag pattern of charge density. The latter one is

$$n_{\text{tr}}(x, t = 0) = \nabla\phi_{c-}(x) + \cos(2k_{FS1/2}x) \exp\phi_{c+}(x) \cos\phi_{c-}(x) \cos\phi_{s-}(x) \cos\phi_{s+}(x) + \cos(2k_{FS3}x) \exp\phi_{c+}(x) \cos\phi_{c-}(x) \cos\phi_{s-}(x) \cos\phi_{s+}(x). \quad (5)$$

As a result the transverse susceptibility  $\chi_{\text{tr}}(x, t) = \langle n_{\text{tr}}(x, t)n_{\text{tr}}(0, 0) \rangle$  shall have small and large components as well:

$$\chi_{\text{tr}}(x, t = 0) = \frac{\langle \nabla\phi_{c-}(x)\nabla\phi_{c-}(0) \rangle}{\pi^2} + \frac{1}{(2\pi)^2} (\cos(2k_{FS1/2}x) + \cos(2k_{FS3}x)) \Pi_{\nu} \exp(\pm\phi_{\nu}(x)\phi_{\nu}(0))^2 \quad (6)$$

where the first term is the  $q = 0$  response and the second is the  $q = 2k_F$  response ( $q$  is the momentum along the chain). The first term describes the charge response to a uniform field (along the chain), the second one the response to a staggered field. The signs in the exponent of the second term depends whether we study the S1/2 or S3 response, but since they are squared they do not contribute to the final answer. The two correlations have strikingly different behavior:

**q = 0:** the expectation value of  $\nabla\phi_{c-}(x)$  correlator is zero as the gapped field cannot fluctuate, or to be more precise  $\phi_{c-}$  is locked at values that minimize the cosine and jumps between these are localized instantons that can be pinned on the lattice. Finite value of this correlator is possible only at finite frequencies.

**q = 2k<sub>F</sub>:** here we expect large susceptibility with a power law decay in real space since *all* four bosonic modes contribute with the gapped fields expectations  $\langle \cos\phi_{c,s-}(x) \rangle = 1$  and  $1/r^{K_{\nu}}$  terms from gapless modes. Upon Fourier transformation we arrive at gapless susceptibility with a broad power law peak  $\sim \omega^{(K_{c+}+K_{s+})/2-2}$  (and the same  $q$  dependence due to Lorentz invariance in this sector).

This dichotomy shall manifest in physical properties of the system. We consider three relevant examples below.

### 1. Peierls instability

The Peierls instability is an effect induced by a lattice distortion which, usually at commensurate fillings, opens a gap in the single-particle spectrum of electrons [7]. Since any single-particle backscattering operator induces bands backfolding into the reduced BZ. The problem is usually solved through Bogoliubov transformation where the ratio between backfolded- and normal-spectral weights is

$$v_q/u_q = \sqrt{\frac{1 - V_P(q)}{1 + V_P(q)}}. \quad (7)$$

coupled to the  $\phi_{c-}$  and we shall focus on its experimental signatures in Sec. IV. Before, we shall compute the relevant observables.

A natural quantity to investigate is the fluctuation of the transverse density operator

$$n_{\text{tr}}(x, t = 0) = \psi_{S1/2}^{\dagger}(x)\psi_{S1/2}(x) - \psi_{S3}^{\dagger}(x)\psi_{S3}(x). \quad (4)$$

Neglecting hybridization, we find that the density has two components, small and large momentum:

Here  $V_P$  is the Peierls potential that is driving the transition, which is inversely proportional to the soft phonon frequency  $V_P \sim 1/\omega_{Q_i}(q)$ .

The transition can also be driven by the electronic part whereby the susceptibility of the electronic liquid softens the phonon dispersion at a given momentum. Let us consider an ion-ion interaction with a contribution mediated by the electronic liquid

$$V_{I-I}(R_i - R_j) = \rho_I(R_i)\rho_I(R_j) + \rho_I(R_i)\chi(R_i - R_j)\rho_I(R_j).$$

The dynamics of a phonon mode at a given wave vector  $q$  are determined by  $\omega_{Q_i}(q) \sim \partial_Q \partial_Q V_{I-I}(Q_j)/\partial^2 Q|_q$  (where  $Q_j$  is the normal coordinate of the  $j$ th mode). If the lattice distortions (a sum of which gives the coordinate  $Q_i$ ) are perpendicular to the silicon step then the  $\chi_{\text{tr}}(q)$  shall renormalize  $\omega_{Q_i}(q)$ , namely:

$$\omega_{Q_i}(q) = \omega_{Q_i}(q)^{(0)} / \sqrt{\epsilon_{RPA}^{(Q_i)}(\omega_{Q_i}(q)^{(0)}, q)} \quad (8)$$

which can be simplified close to the pole where  $\epsilon_{RPA}^{(Q_i)}(\omega_{Q_i}(q)^{(0)}, q)$  is dominated by the  $\chi_{\text{tr}}(\omega_{Q_i}(q)^{(0)}, q)$ . For  $q \approx 2k_F$  we can now predict a substantial mode softening that will lead to a Peierls transition based on the previous relations  $V_P \sim \sqrt{\chi_{\text{tr}}(\omega_{Q_i}(q)^{(0)}, q)}$ . For Au-Si(553), such a softening of the phonon modes, in the vicinity of gold atoms, and the appearance of symmetry prohibited modes, due to the presence of a zigzag CDW, is in full agreement with a very recent Raman study [29].

It is interesting to note that if *all* four bosonic modes would be gapped, then the self-correlation of the backscattering operator does not decay in real space. Hence, after Fourier transforming  $V_P(q) = V_0\delta(q)$ —a very strong softening but only at commensurate fillings (only a perfect nesting) is permitted. In our case, where only *half* of bosonic modes is gapped there is a decay in real space

$$\chi_{\text{tr}}(r)|_{(q \approx 2k_F)} \sim r^{(K_{c+}+K_{s+})/2-2} \quad (9)$$

which, in turn, leads to a broadening of the peak—the presence of gapless modes implies that the transition may take



place slightly away from the Fermi surface; an imperfect nesting is permitted. The transition can take place either in the vicinity of  $2k_{FS1/2}$  or  $2k_{FS3}$  but, since the former one is quite close to half-filling, we predict the bands backfolding to be present close to the  $k_{FS1/2}$  Fermi points.

In the case of imperfect nesting, the effective strength of the Peierls potential  $V_P$  is proportional to the bare periodic potential caused by a tiny lattice distortion (e.g., dimerization) times the Fourier transform of  $\chi_{tr}(r)$ . We now assume that the bare strength of the Peierls potential  $V_P^{(0)}$  does not depend on temperature.<sup>4</sup> In the standard perfectly nested Bogoliubov scenario, we then expect no temperature dependence of  $v_q/u_q$ . However in our problem of partial nesting, there is one more source of the temperature dependence; it comes from the correlation function  $\chi_{tr}(\omega_{Qi}(q)^{(0)}, q; T)$ . For the TLL, these correlations are known exactly and can be expressed in terms of the *Beta*  $([\pm V_v q + \omega]/T; K_v)$  functions. To be precise, for a given incommensurability  $q = 0.04$ , with the knowledge of lowest temperature  $v_q/u_q$  we can estimate  $V_P$ . Then, since the temperature dependence of susceptibility  $\chi_{tr}(\omega_{Qi}(q)^{(0)}, q; T)$  is known, we can test our CDW scenario. We shall compare this idea with the ARPES experiments seeing a backfolding there, see Sec. IV.

## 2. Transverse dielectric constant

To analyze the properties of the entire stepped silicon surface, it is of interest to compute the interedge Coulomb interaction with the metallic two-leg ladder (from Au sites and their vicinity) in between. We need to find the dielectric constant of the metallic system around the Au atoms. We probe with the electric field in between two edges, hence perpendicular to the direction of the two-leg ladder, and are interested in the response to the transverse electric field. We are interested in the local response and assume that the two charges are localized and the field is strictly perpendicular. Their relative position is  $\vec{r} = \{x, y\} = \{0, d_{\text{step}}\}$ . We then need to sum both small and large momentum components

$$V_{\perp}(x=0) = \frac{V_{\text{Coul}}(q=0)}{\epsilon_{tr}(q=0)} + \frac{V_{\text{Coul}}(q=2k_F)}{\epsilon_{tr}(q=2k_F)}$$

with  $\epsilon_{tr}(q) = 1/(1 + \chi_{tr}(q))$ . The large momentum component of  $V_{\text{Coul}}(q)$  is usually small and here it is further suppressed by large susceptibility from Eq. (6). On the other hand the small momentum component can be large and has two distinct regimes: It is basically unscreened in the low frequency limit ( $\omega < \Delta_{c-}$ ) but the screening suddenly kicks in and suppresses the  $V_{\perp}(q \approx 0, \omega > \Delta_{c-})$  at larger energies where harmonic oscillations of the  $\phi_{c-}$  field are allowed. In the low energy regime, the expectation value of the correlation  $\chi_{tr}(q)$  is zero as the gapped field cannot fluctuate. To be more precise,  $\phi_{c-}$  is locked at values  $0 \pm n\pi$ ,  $n \in \mathbb{N}$  that minimize the cosine. The textbook formula 21.31 in Ref. [45] expresses this physics and reveals that there is a gap  $2\Delta_{c-}$  in the susceptibility. This statement relies on the pure 1D character of the system and one should inquire if it still holds upon when including interstep Coulomb interactions shown in Fig. 4. For

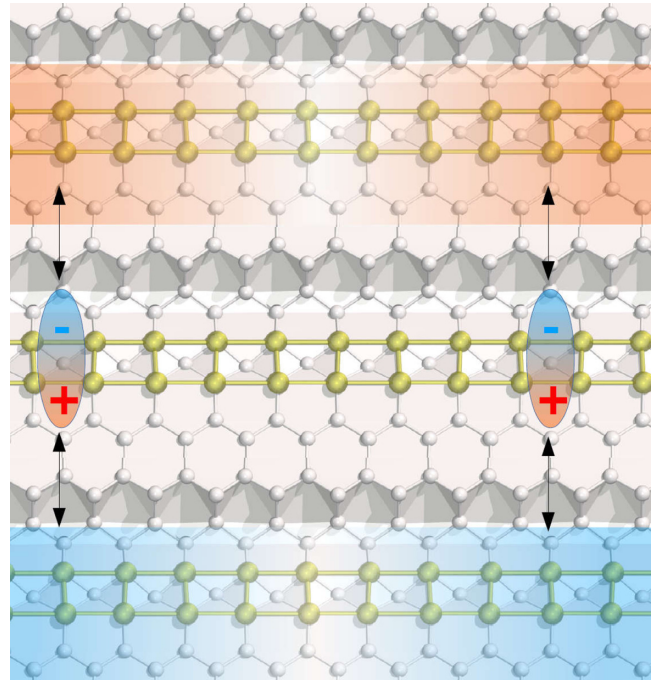


FIG. 4. A schematic picture of an interstep dipole interaction  $V_d$  that allows us to couple the  $\phi_{c-}$  solitons with gapless holons from neighboring 1D systems. We see two solitons on the step that would usually not interact, but now each of them can induce charge fluctuations in the neighboring steps. We then have an analog of RKKY coupling mediated by gapless holon propagators. This is a charge interaction and so it does not apply to  $\phi_{s-}$  excitations for which the respective solitons remain fully nondispersive.

Au-Si(553), these types of interactions were also postulated in a recent experimental study [28]. An answer to this question is given in Appendix C, where the procedure to compute the first approximation to  $\chi_{tr}(q)$  is given.

The result of this calculation is shown in Fig. 5. We show that even in this relaxed 1D scenario, the amount of two-body spectral weight at low frequencies is very small; it may raise up to finite values already at temperatures  $T \approx \Delta_{c-}/2$ . Let us remind that for Au-Si(553),  $\Delta_{c-} = 7$  meV.

## 3. Single-particle propagator: Spectral function

This behavior of the two-body susceptibility (at  $q \approx 0$ ) should be contrasted with a single-particle propagator. The expression for the Greens function in bosonization representation contains all fields  $\phi_v$  and  $\theta_v$  which is the reason why it has much milder singularity; each power law there is weakly divergent with an exponent  $\sim (K_v + 1/K_v)/2$ . Furthermore, the gapped fields are convoluted with gapless ones and the correlation function of the gapped ones is proportional to  $K_{1/2N}(x)|_{N=2}$  whose Fourier transform is less singular than that of  $F[K_0(x)]$  for the  $\chi_{c-}$  susceptibility (here  $K_v$  is a modified Bessel function of the second kind). To obtain a quantitative prediction for the spectral function, we can use the result of Ref. [49] by noticing that both, charge and spin sector, have one mode gapped and the other gapless. The gaps are identical and under the assumption that spin and charge velocities are equal. Then the total spectral function will be an autoconvolution  $\tilde{A}t[A_{nu}](\omega) = A_{c+,c-}(\omega) \otimes A_{s+,s-}(\omega)$ . Here

<sup>4</sup>Publication in preparation.



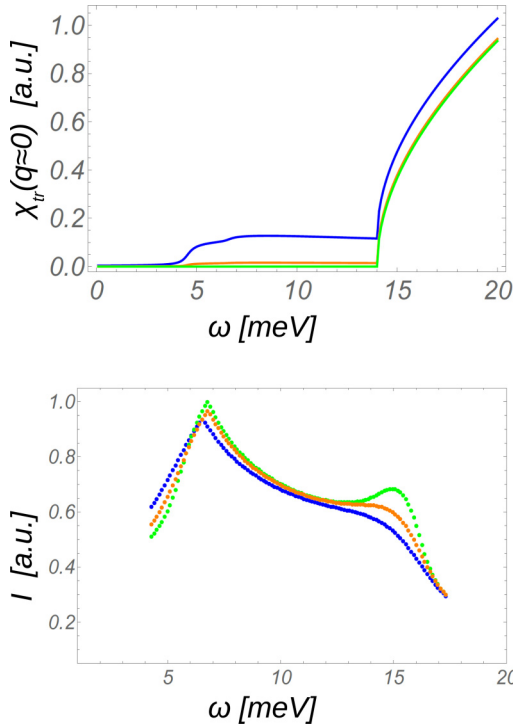


FIG. 5. Top panel: transverse susceptibility  $\chi_{tr}(q \rightarrow 0, \omega)$  showing a large gap up to  $2\Delta_{c-}$  which inhibits the screening of Coulomb type interactions, even when the in-gap “beyond-1D” processes shown in Fig. 4 are included at  $T = \Delta_{c-}/2$ . Bottom panel: single-particle spectral functions  $A(\omega, q = 0)$ . Blue and green are spectral functions at  $T = \Delta_{c-}/6$  and  $T = \Delta_c/2$ , respectively. Despite the gap in the two bosonic modes, we expect finite spectral weight at the Fermi energy. In both panels, the  $\Delta_{c-}$  is chosen to be 7 meV. We observe that even upon moving from a pure 1D model to a 2D situation, by the consideration of the  $V_i$  interaction, the two-body susceptibility has a substantial gap, while in the single-particle spectral function (even without the  $V_i$ ), the gap is not pronounced.

$A_{c(s)+,c(s)-}(\omega)$  contains one massive and massless mode, the amplitude of the massive sector is known and can be expressed as a sum of terms (where each term corresponds to single, double... soliton excitation of the gapped part):

$$A_{c(s)+,c(s)-}(q, \omega; \Delta_i) = \frac{(Z_2 \sqrt{\pi} \Delta_i)}{(2\pi)^3} \int_{-\infty}^{\infty} dz \exp\left(\frac{z}{2}\right) \times [\Pi(\Delta_i \cosh(z) - \omega, \Delta_i \sinh(z) - q) + \exp(\Delta_i \cosh(z)/T) \Pi(\Delta_i \cosh(z) + \omega, \Delta_i \sinh(z) + q) + \{\omega \rightarrow -\omega, q \rightarrow -q\}] \quad (10)$$

where the gapless single-particle “polarizability” reads:

$$\Pi(\omega, q; T_i) = \left(\frac{1}{2\pi^3}\right)^{1/2} \left(\frac{2\pi}{\Delta_i}\right)^{\gamma} T_i^{\gamma-3/2} \times \Re \left[ B\left(\frac{\gamma+1}{2} + \frac{i(q+\omega)}{2\pi T_i}, 1 - \frac{\gamma+1}{2}\right) \right] \times \Re \left[ B\left(\frac{\gamma}{2} + \frac{i(\omega-q)}{2\pi T_i}, 1 - \frac{\gamma}{2}\right) \right] \quad (11)$$

where the gapless TLL Green’s function exponent for a single chain is known, for instance for the charge part  $\gamma_c = (K_{c+} + 1/K_{c+})/2 - 1$ . To obtain  $A_{c(s)+,c(s)-}(\omega)$  we need to integrate the above formula over momenta. Here we assume that the 1D result holds because deviations from pure unidimensionality are primarily through interactions and not by single-particle hybridization. The main conclusion from this section is that the partial gap, namely the gapping of two out of four TLL modes, itself will not be visible in single-particle probes but can nevertheless substantially affect *selected* two-body susceptibilities.

#### IV. EXPERIMENTAL REALIZATION OF THE NEW THEORY IN Si(553)-Au

In the preceding theoretical part, we found that the Rashba-split + interactions causes a gap in the susceptibility of the two-leg ladder while the single-spectral function keeps a finite weight near  $E_F$ . The experimental part of our work, performed on the specific Si(553)-Au system, will be built around a critical analysis of the Peierls-physics indicators. Since it is experimentally hard to detect changes in the spectral function  $A(q, \omega)$ , one needs to search for other means of detection. An indirect method is by quantifying the temperature dependence of backfolding in ARPES. Furthermore, we postulate that antisymmetric pinning, either by changing the position of the Au-add-atoms or by incorporating periodic defects, can massively increase the CDW instability of the system *related to coupled edge-step solitons*. The theory expects at low  $T$  the charge on the Au chain to be distributed in a zigzag pattern and the existence of solitons on the Au chain which react with the charge on the Si-step edge. We will here discuss here results of our STM measurements [26,50]. Details of the experiment are described in the Appendix.

##### A. Change of the back folding with T

To confirm the electronic driven CDW-like instability it is important that the backfolding intensity in ARPES changes with  $T$ . Figure 6 shows the backfolding in the 3rd.  $\times 2$  Brillouin-zone<sup>5</sup> as measured by ARPES. Shown are measurements at low- $T$  ( $T = 50$  K) and high- $T$  ( $T = 260$  K). Besides broadening by temperature, a change of the backfolding intensity is clearly visible. The momentum distribution curve at the chemical potential (red curves) allow us to quantify a reduction of about 50% of the backfolding when going from low- $T$  to high- $T$ . This, together with known results from low-energy diffraction (see, e.g., Refs. [16,20,42]) shows therefore signatures of a Peierls-like CDW instability. We compare this with the theory of Sec. III B 1: Using the experimental result of the backfolded intensity, see Fig. 6(a), the low energy value of the ratio  $v_{0,04}/u_{0,04}|_{T=50\text{ K}} = 0.38$  allows us to fix  $V_P = 0.077$ . With  $K_v = 0.5$  (a value appropriate for weak long-range interactions), we obtain  $v_{0,04}/u_{0,04}|_{T=260\text{ K}} = 0.165$  a value close to the experimental result.

<sup>5</sup>As already visible in Fig. 1, this 3rd.  $\times 2$  Brillouin-zone has a better visibility of the  $\times 2$  folding. This is most likely a BZ-selection effect (cf. Ref. [55]) caused by the fact that the true surface unit cell is the  $\times 6$  BZ.

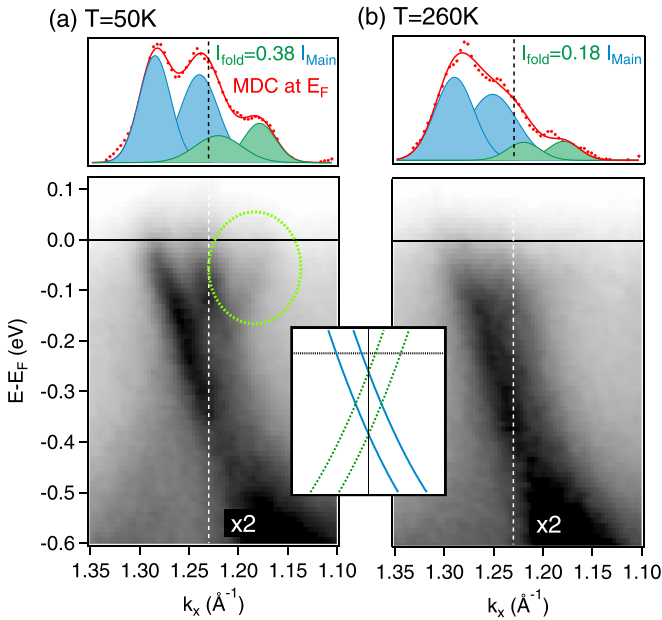


FIG. 6. ARPES measurements for (a) low ( $T = 50$  K) and (b) high temperatures ( $T = 260$  K) showing the change of the  $\times 2$  backfolding with temperatures. The lower panels shows the photoelectron intensity maps along the same direction as indicated in Fig. 1 (c) near the 3rd.  $\times 2$  BZ. The backfolding bands can be well seen at  $T = 50$  K in the region encircle by the light green lines. Compare also with the schematic band situation drawn the inset between the lower panels where the original bands are blue and the replica bands are green (see also Ref. [18] for details like the hybridization between original and replica bands not addressed in this schematic). The top panel shows the momentum distribution curves at the chemical potential together with a line fit to quantify the change in backfolding replica intensities (in green). Clearly, the replica intensity reduces with temperature.

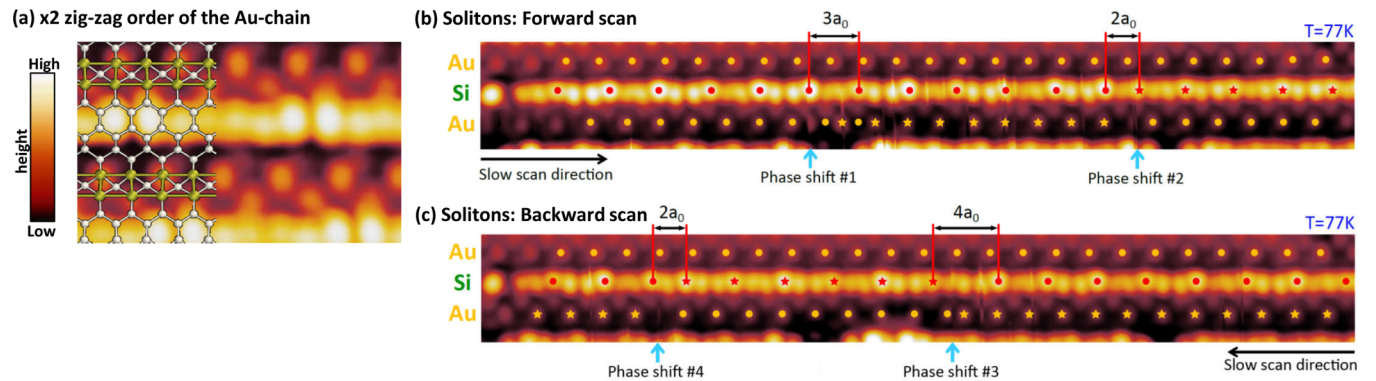


FIG. 7. (a) Measurements to show that the Au ladder follows a zigzag pattern [26,50]. STM images of the unoccupied states of the Si(553)-Au surface at tunneling biases of  $U = +0.2$  V ( $T = 77$  K). The structural model of Ref. [12] is overlaid. The charge clouds on each bar shows a  $\times 2$  periodicity. The order between the two bars of the ladder follows a zigzag pattern. The measurements in (b) and (c) show that solitons are visible as change of register in the otherwise periodic charge pattern of the Au sites [26]. STM constant current images ( $U = +0.3$  V) of a single spin chain and two surrounding Au chains, comparing two subsequent images with opposite line-feed direction. In particular, the fast scan direction is vertical, i.e., the slow scan movement is horizontal as indicated by the black arrows. The Au chain exhibits several phase shifts as marked with the cyan arrows. Most Au chain phase shifts come hand in hand with a phase shift in the Si-step-edge chain as indicated by the red symbols. Red stars represent one configuration and red dots the other configuration.

## B. Zigzag pattern on the Au chain

As described in the beginning of Sec. III B, an immediate implication is that charges on the ladder should have a high propensity to form a zigzag pattern. This additional many-body part of susceptibility should be incorporated in DFT computations of this compound and should then manifest in STM measurement. Figure 7(a) displays a high-resolution STM constant current image at 77K with bias of  $U = +0.2$  V. It is part of a bias-dependent series already published in Ref. [50]. It shows two Si edges and two Au chains in between. The steps lead upwards to the top of the page. The structural model of Ref. [12] is overlaid and helps us to identify two contributions, one bright horizontal feature stemming from the Si edge and a series of characteristic circular charge clouds from the Au chains. At this bias, the bright Si-step-edge shows  $\times 6$  periodicity as discussed in Ref. [50] and in line with the correct surface Brillouin zone. At higher bias, the Si-step-edge displays the well-known  $\times 3$  superstructure [50]. The circular charge clouds of the Au chains show a  $\times 2$  spacing on each bar of the ladder. The two bars are ordered in a zigzag fashion, i.e., the pattern on each of the two bars of the ladder is shifted by one lattice constant to the right. The charge-cloud on the upper bar (lying below the next step) is always more defined whereas the charge clouds of the lower bar have a more asymmetric shape; they connect to the Si edges and are weaker.

## C. Solitons in the Au chain

Now that we have shown the presence of the zigzag pattern, we can search for its characteristic excitations. Remarkably, the theory given by Eq. (3), the sine-Gordon theory, has characteristic soliton-type excitations that can be unambiguously observable in real space, in the temperature range of around  $T = 77$  K where the experiments were done. Hence, a

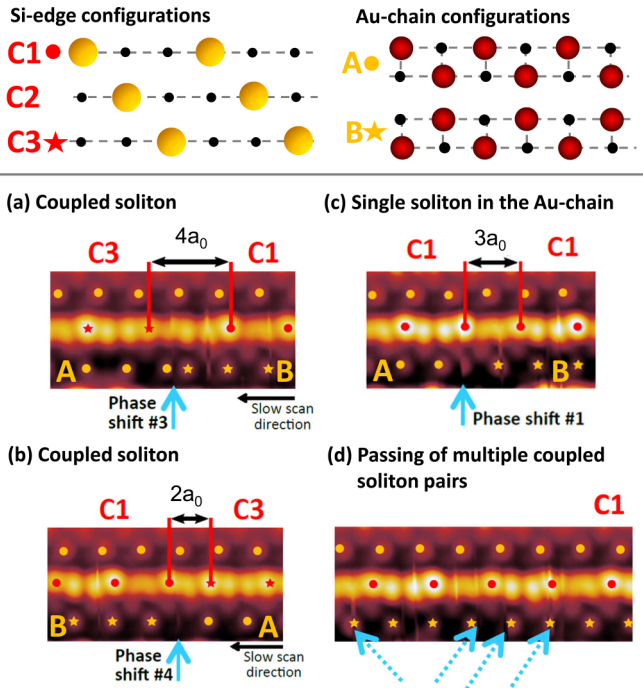


FIG. 8. Top panel shows the different configurations possible for the Si-step-edge (C1,C2,C3) and Au-chain (A,B). (a),(b) Coupled Au-chain and Si-step-edge soliton passing. Slow scan direction is from right to left as marked by the black arrow. In (a), at phase shift #3 the Au-chain's phase changes from B to A and the Si-step-edge configuration from C1 to C3. At phase shift #4 in (b), the Au chain's phase changes from A to B and the Si-step-edge configuration from C3 to C1. The Si-step-edge soliton observed in (b) is the antisoliton of the spin chain soliton observed in (a). (c) Single Au-chain soliton passing. No phase shift in the Si-step-edge chain is observed. (d) Multiple passings of coupled soliton pairs. A passing of coupled soliton pairs does not change the Si-step-edge phase at larger distances as marked by the red dots.

strong signature of the many-body character of the electronic liquid under our investigation may then come from the fact that the lowest-lying excitation of the system (of the  $\phi_{c-}$  mode) is a soliton (the low energy, in-gap threshold shown in Fig. 5). This peculiar nonlinear particle reveals an underlying sine-Gordon Hamiltonian. We then embark on its search. Figures 7(b) and 7(c) display two STM constant current images at 77 K. The bias of  $U = +0.3$  V has been chosen to be sensitive to the unoccupied DOS of the Au chains as well as to the Si-step-edge atom. In the images of Figs. 7(b) and 7(c), the step edge is surrounded by two Au chains, see labels in Fig. 7. One Au chain resides on the same terrace as the step edge, the other chain on the terrace below. Both chains exhibit the characteristic circular charge clouds discussed above with  $\times 2$  spacing. To distinguish the different configuration of the Au chain, see also Fig. 8, the Au-charge clouds are marked by orange dots for configuration A and stars for configuration B.

Both images in Figs. 7(b) and 7(c) display the same surface area (see, e.g., the defect present for both at the left end of the chains). The images were taken in quick succession, one after the other. They differ by the choice of slow scan direction of the tunneling tip: (b) was scanned from left to

right (forward scan) and (c) from right to left (backward scan). Focussing on (b), the cyan arrows mark positions at which the phase of the lower Au chain suddenly shifts. Some parts of the STM image display domain A (orange dots) while others display domain B (orange stars) of the Au chain. While the orange dots of domain A coincide with the Au-charge clouds on the left of the phase shift, they are in between the Au-charge clouds on the right of this phase shift, domain B (orange stars). This observation indicates the presence of a single soliton, which has propagated through the Au chain during the STM measurement, and, thereby, shifted its phase by  $a_0$ . It is noteworthy, in order to diminish the effect being an experimental artifact, that only the lower Au chain shows signatures of passing solitons and not the upper one.

#### D. Coupled solitons

So far, we have shown that Coulomb interaction between the edges should be unscreened, because the  $\phi_{c-}$  mode is locked prohibiting any variations of the transverse electric field. By the same argument applied at finite temperature, one can say that the presence of the soliton modifies locally the electrostatic potential landscape, see Fig. 4. So far we have not considered the carriers on the edge of the silicon step, being beyond our current theory. However, we know that they exist, we can observe them in STM, so we can use them as a probe of the local potential. One can then directly inspect if the scenario proposed in Fig. 4 is correct by checking if Au solitons are accompanied by any charge variations on the Si-step edge.

Indeed, our STM provide direct evidence for a coupling of the solitons [26]. As visible in Figs. 7(b) and 7(c), many Au-chain phase shifts come hand in hand with a phase shift in the Si-step-edge chain. The configuration of the Si-step-edge chain is encoded in the red symbols where the red dots represent the configuration C1 and stars configuration C3, see left top of Fig. 8. Remarkably the solitons are mobile as we see a change of the pattern between the two STM scans along the chain (slow scanning direction). In comparison to the confined solitons in Si(111)-In  $4 \times 1$  (see, e.g., Refs. [51,52]), it is noteworthy to mention that the solitons in Si(553)-Au are deconfined [26]. Only this allows the observation of a single, mobile soliton.

Figure 8 shows in detail some characteristic soliton passings. Figures 8(a) and 8(b) show Au-chain solitons coupled to solitons on the Si-step-edge. Looking onto (a) at phase shift #3, the Si-step-edge shifts from configuration C1 to configuration C3 (the scan direction was right to left). The difference in pattern of the Si-step-edge is  $4a_0$  at the phase shift, i.e., a shift of  $-a_0$ . At the same time on the lower Au chain, the configuration changed from B to A accompanied by a phase shift of  $+a_0$  for the Au chain. Looking onto (b) at phase shift #4, the Si-step-edge shifts from configuration C3 to configuration C1 with a shift of  $+a_0$ . The Au chain changed from A to B with a phase shift of  $-a_0$ . The soliton in (b) may be considered the antisoliton of (a).

Also other solitons events are visible. Figure 8(c) displays an Au-chain soliton which is not accompanied by a Si-edge soliton. Finally, Fig. 8(d) indicates several soliton pairs propagating through the Au chain. At the locations indicated by



the cyan arrows, the phase of the Au chains appears to change for a short time (approximately one second) before flipping back to its initial configuration; The same seems to happen for the Si edge, as the the Au-chain phase shifts seem to be accompanied by short, spikelike intensity changes at the Si edge. As expected for soliton pairs, their numerous passing does not alter the Si-edge configuration at larger distances—resulting in regular  $3a_0$  patterns.

## V. DISCUSSION

### A. The mechanism

In the course of this study, we investigated the effect of Rashba splitting on the electronic structure of the two-leg ladder by bosonization within a TLL model and subsequent renormalization group analysis. We were able to show that, when we reach the characteristic Rashba-split length, it modifies the RG flow and lifts the “frustration” related to the pinning of canonically conjugated fields of densities and their momentum. As a result, two out of four TLL modes (namely the both transverse charge and modes,  $c-$  and  $s-$ ) open a spectral gap ( $\Delta_{c-}$  and  $\Delta_{s-}$ ) which is determined by the energetic size of the Rashba splitting.

Interestingly, there is a dichotomy. We found that the gapping of two out of four TLL modes itself will be hardly visible in the single-particle probes, i.e., *not* in the spectral function as probed by ARPES. Nevertheless, we have shown substantial influence on the electronic two-particle properties of the electronic liquid, i.e., in its susceptibilities. These shall reveal themselves through direct and indirect effects. The direct effect is a two-body phenomenon, deducible from Eq. (3), resulting in a rather exotic spin order. The indirect effect, caused by the modified dielectric function, is a backfolding of the  $S1/2$  bands; it is a Peierls-type phenomenon but for an incommensurable nesting. These two effects support each other: Once the imperfect nesting triggered the backfolding, there is a small spectral weight that enjoys interaction through the large, unscreened (note the behavior of dielectric function)  $q = 0$  component of Coulomb interactions.

Any charge modulation may produce a staggered component of the relevant two body interaction  $g_{2c}$ . Through an operator product expansion it can be shown [53] that this leads to an emergent single-particle “Peierls” backscattering term of the form proposed in Sec. III B 1. This self-consistency implies that, even if the initial lattice does not support the Peierls term, it will appear through spontaneous symmetry breaking. It should be noted that the instability promoted by  $g_{2c}$  can break spin-rotational invariance and so the additional Peierls backscattering may involve an in-plane spin precession. So, while nominally Peierls backscattering with a spin flip may appear like an unusual concept, such a process can be dynamically generated in higher orders. As a result a substantial enhancement of backfolded spectral weight should be visible even if the momentum conservation demands a spin-nonconserving  $S1 \rightarrow S2$  process.

### B. Experimental platform

Our theoretical reasoning is tested on the Au-Si(553) system. Our experiments show that (i) indeed there is a tem-

perature dependence of the backfolding visible in ARPES and (ii) apart from a symmetric CDW, there is a zigzag pattern of charge density visible in the STM showing the importance of a staggered component of susceptibility. Furthermore, at finite temperature  $T \approx \Delta_{c-}/2$ , the regular zigzag pattern is disrupted by local steplike excitations. Using STM, we found clear experimental signatures of solitons. Although our experimental signatures are only indirect it should be noted that they are hard to reconcile with any other theoretical scenario. The solitons, the abrupt changes of the order’s register, are an excited eigenstate for the 1D theory of a collective nonlinear liquid, while single-particle theories would support only plane waves type excitations. We do expect that this 1D theory can be corrupted by the interstep long-range interactions. Thus we computed the influence of such quasi-2D interactions, proving that, at this level of treating the dimensional crossover, the solitons remain as proper eigenstates and should be indeed observable. However, one now has to account for interactions between them. These interactions reduce the dichotomy between single-particle Green’s function and the susceptibilities but are not capable to erase it. Consequently, our experiments have shown the Au-chain solitons interacting with the Si-edge solitons but without destroying the overall zigzag ordered state of the Au chain.

A direct experimental proof of the existence of a partial, only transverse spectral gap may be more difficult to obtain. To this end one can try to employ the partial but mutual locking of spin and charge fluctuations. We can focus here on the nuclear quadrupole resonance since Au nucleus has spin greater than 1; the off-centered Au sites<sup>6</sup> should show a NQR resonance of the transverse quasiantiferroelectric configuration coupled with in-plane magnetism. The antiferroelectric zigzag pattern induce local electric field gradient and quadrupolar states split is further enhanced by magnetic environment. Interchanging some of the Si atoms with Ge is even a more sensitive probe as Ge has quite a high nuclear moment. Another (experimentally quite demanding) option to probe the slowly oscillating anisotropic magnetic order is to use positron spin-polarized muon spectroscopy. Finally, one can try to couple the spin currents flowing in the system with an external fluctuating magnetic field in a lock-in manner with an STM experiment measuring the amplitude of the competing CDW order. This last option is particularly exciting as it would be the first detection of such a magneto-CDW coupling.

We emphasize an important limitation of our model. Our reasoning is based on the assumption that the effective single-particle hybridization between the carriers of the Au chains on the neighboring steps cannot destroy the 1D fermionic Tomonaga-Luttinger liquid. Such process would drive a dimensional crossover, at energy scales larger than  $\Delta_{c-}$ . However, in this paper, we show that two bosonic modes develop a 7 meV gap each which leads to an upper bound of the bare (DFT) interchain-hopping hybridization of 80 meV

<sup>6</sup>These should have the largest field gradient. However, unfortunately there is also a constant surface electric field gradient, possibly with a transverse component. This gradient causes Rashba splitting and needs to be separated out.

for which our 1D model remains valid.<sup>7</sup> If we assume that the coupling is indirect and goes through carriers on the Si edge, then any disorder on the edge will raise this upper bound to even higher values. Since our findings are corroborated by experiments, it suggests that the edge carriers have some very unusual character that indeed keeps them away from delocalization. This assumption will be confirmed by a subsequent experimental paper dedicated to these states [54].

We can also build links with other studies of the system. Our theory allows us to predict the strength of the Coulomb interaction between the carriers on the Si-step-edges. This also implies a curious interconnection: doping of the Si edge (these extra local charges manifest as solitons) changes the screening on the terrace; therefore the Au-atoms' dimerization will change. This is an alternative many-body interpretation of the experimentally observed effects where a single-particle phenomenology was proposed in Ref. [43]. Recently we became aware of *ab initio* work of Braun *et al.* [27]; based on our results we see that the tentative relation between modified dimerization of Au atoms and a modified energy landscape of dangling bond, that have been indeed numerically detected therein, is not a trivial effect of charge transfer but, instead, is a phenomenon deeply rooted in a many-body susceptibility of the electronic liquid on the Si-step-edge.

## VI. CONCLUSION

The theory of two-leg ladders is a well-developed field, but a phase where precisely half of the modes (the transverse modes) are gapped has not been ever predicted before. Our mechanism, which can be called Rashba incommensurability, exists in a so-far-unexplored regime where the strength of the Rashba split is comparable to the weak backscattering interactions while the forward-scattering interactions are strong.

Our highly nonobvious result of many-body theory causes exotic properties, for instance, intermixing of spin density wave magnetism and the zigzag Peierls CDW; an increase in the amplitude of one transverse mode will inevitably increase the other. Specifically, instead of a fully developed magnetic order, we have an incipient magnetism; because already half of the magnetic fluctuations are frozen, further perturbations, such as impurities, could stabilize the magnetism.

Also, we demonstrate a curious *dichotomy*: While the spectral gap opening is only very weakly pronounced in the single-particle spectral weight, it is fully visible in selected two-particle properties, e.g., the transverse susceptibility. Due to this peculiar combination of correlation functions, a Peierls-type backfolding can occur despite the slightly incommensurable nesting conditions.

On the experimental side, we were able to substantiate our findings in the Au-Si(553) surface system. We showed that the temperature dependence of the backfolding is in agreement

with our imperfect nesting scenario. The direct observation of soliton excitations is a hallmark of the 1D sine-Gordon model.

It should be emphasized that our findings are not restricted to the specific experimental realization discussed here but can be seen as a more general blueprint; the Rashba effect is just one manifestation of a symmetry breaking at the surface. *Any* symmetry-breaking term can be sufficient to induce a slight incommensurability between Fermi points. This, in turn, is sufficient to break the degeneracy of scattering channels and to induce partial gaps. We thus expect that the mechanism proposed here will occur commonly in artificially created low-dimensional systems at surfaces.

## ACKNOWLEDGMENTS

We gratefully acknowledge financial support from the Deutsche Forschungsgemeinschaft (DFG) in the research unit FOR 1700, project Scha1510/4-1. Additional DFG funding was provided within Germany's Excellence Strategy through the Würzburg-Dresden Cluster of Excellence on Complexity and Topology in Quantum Matter ct.qmat (EXC 2147, Project ID 390858490).

## APPENDIX A: EXPERIMENTAL

### 1. Sample preparation

The preparation was similar to that in Ref. [50]. We used *n*-doped (phosphorus) Si(553) substrates. The samples were cleaned in an ultrasonic bath with acetone, isopropanol, and methanol of highest purity for 2 min in each solvent, after the protective photoresist was removed with standard grade acetone. To avoid residual solvents the samples were blown off with dry nitrogen. The base pressure of the UHV chamber used for the *in situ* preparation was below  $5 \times 10^{-10}$  mbar. After degassing the samples, we heated up to 1250 °C via direct current heating to remove the protective oxide layer. Au evaporation of 0.48 ML was performed while the substrate was held at a temperature of 650 °C, followed by a short post annealing at 850 °C. The quality of the preparation was controlled by LEED.

### 2. ARPES

Photoemission measurements were performed with a SPECS Phoibos-100 electron analyzer and a 6-axis SPECS Carving goniometer. We used a nonmonochromatized He-discharge lamp optimized for the He-I line ( $h\nu = 21.22$  eV). The energy resolution was set to 25 meV. To guarantee defect free samples, we performed a thermal refresh procedure similar to the post annealing step prior to ARPES measurements.

### 3. STM

STM measurements have been performed with a low-temperature STM instrument from Omicron at a sample temperature of 77 K. All STM images presented have been recorded in constant current mode using a PtIr tunneling tip.

<sup>7</sup>This bound is in the initial high-energy (so called UV) limit of the renormalization group (RG): If we start a many-body RG procedure from the result of a DFT calculation as an input, then, provided the initial input is  $t_{\text{perp}} < 80$  meV, the  $t_{\text{perp}}$  will be renormalized by interaction down to  $t_{\text{perp}} < 14$  meV and the gaps of two bosonic modes will prohibit such single particle hopping.

## APPENDIX B: UMKLAPP

If the two-leg ladder is commensurate, additional Umklapp terms appear in the Hamiltonian:

$$\begin{aligned}
 H_{\text{umk}} = & g_{3\parallel} \int dr \cos(2\phi_{s+}) \cos(2\phi_{c+} + \delta x) \\
 & + g_{3a} \int dr \cos(2\theta_{s-}) \cos(2\phi_{c+} + \delta x) \\
 & + g_{3b} \int dr \cos(2\phi_{s-}) \cos(2\phi_{c+} + \delta x) \\
 & + g_{3c} \int dr \cos(2\phi_{c-}) \cos(2\phi_{c+} + \delta x). \quad (\text{B1})
 \end{aligned}$$

Since these terms oscillate with  $\delta$ , their influence becomes important only when the doping  $\delta$  is smaller than the on-shell distance from  $E_F$ . Mathematically, in the RG flow of these Umklapp terms each of  $\partial g_{3i}(l)/\partial l$  is multiplied by a doping dependent coefficient  $J_0(l\delta)$  where the Bessel functions  $J_0(l\delta)$  for small  $l\delta$  may be approximated by one and for large  $l\delta$  by zero. One deduces that when  $l\delta \approx 1$  then the RG flow should stop. In our problem, although these terms are highly relevant (especially the last one) because  $K_{c+} < K_{c-} \ll 1$ , their initial amplitudes are extremely small as they are processes with by far the largest momentum exchange. Hence they are not the dominant perturbations. Furthermore their RG flow will be terminated at some point by finite incommensurabilities present in the system with  $g_{3b}$  flowing the longest as S1/2 are relatively close to half filling. We then expect that the main influence of the terms in Eq. (B1) will be to reduce values of  $K_{c-}$ ,  $K_{s-}$ .

## APPENDIX C: CALCULATION OF INTER-1D CORRECTION TO TRANSVERSE SUSCEPTIBILITY

To validate this last assertion in the realistic system, we shall now compute the  $\chi_{\text{tr}}(\omega, q \rightarrow 0)$ , in the presence of

interstep Coulomb interaction terms that can take us away from the pure 1D picture and potentially destroy the simple picture given above. For low frequencies there are in-gap excitations of the gapped  $c-$  mode: solitons, and potentially also their bound states—breathers. These can be imagined as localized jumps (instantons) between the minima of cosine, heavy particles that can be pinned on the lattice. The energy of these in-gap soliton-type excitations is known  $m_{\text{sol}} = \sin(\pi/4)\Delta_{c-}$ . However, due to strict energy-momentum conservation, they are not allowed to interact. In the TLL theory, they will not couple with the other, gapless bosonic modes.

Nevertheless, the  $\phi_{c-}(x)$  solitons can entertain long-range dipole-dipole interaction  $V_d(\vec{r})$  and then share energy momentum with (and through) gapless excitations on the *other* steps. This is illustrated in Fig. 4. In this way, the strict integrals of motion for a purely 1D system can be violated. We assume the following mechanism: Through the interaction  $V_d(\vec{r})$ , the solitons interact with charged holons  $c+$  from the other terrace and then these are able to excite fluctuations of the gapped  $\phi_{c-}$  field. The susceptibility of the gapless field is known  $\chi_{c+}(\omega) = \text{Re}[\text{Beta}(\omega, K_{c+})\text{Beta}(\omega, K_{c+})]$  as well as the gapped mode temporal fluctuations giving  $\tilde{A}_{c-}(\omega) = F[K^2(t\Delta_{c-}/kT)]$ . The overall interaction is a convolution of the two and shall allow for soliton dispersion—a variation of its energy around the central peak. The above effect of weak soliton dispersion cannot occur for a lone excitation but instead requires a finite density, hence the temperature dependence from  $n_B(m_{\text{sol}}/kT)$  enters in front the amplitude. By computing this additional contribution to  $\chi_{\text{tr}}(\omega < 2\Delta_{c-}, q \rightarrow 0)$ , the  $\chi_{\text{tr}}^{\text{inter}}(\omega > m_s, q \rightarrow 0) = V_d(\vec{r})\tilde{A}_{c-}(\omega)\chi_{c+}(\omega)$ , we can assess if these interstep interaction can significantly contribute to the screening at finite temperatures.

- 
- [1] T. Giamarchi, *Quantum Physics in One Dimension* (Oxford University Press, Oxford, 2004).
  - [2] D. Sánchez, L. Serra, and M.-S. Choi, *Phys. Rev. B* **77**, 035315 (2008).
  - [3] J. R. Schaibley, H. Yu, G. Clark, P. Rivera, J. S. Ross, K. L. Seyler, W. Yao, and X. Xu, *Nat. Rev. Mater.* **1**, 1 (2016).
  - [4] P. Chudzinski, *Phys. Rev. B* **92**, 115147 (2015).
  - [5] F. D. M. Haldane, *J. Phys. C: Solid State Phys.* **14**, 2585 (1981).
  - [6] R. Egger and A. O. Gogolin, *Eur. Phys. J. B* **3**, 281 (1998).
  - [7] G. Grüner, *Density Waves in Solids* (Addison-Wesley, Reading, MA, 1994).
  - [8] P. C. Snijders and H. H. Weitering, *Rev. Mod. Phys.* **82**, 307 (2010).
  - [9] L. Dudy, J. Aulbach, T. Wagner, J. Schäfer, and R. Claessen, *J. Phys.: Condens. Matter* **29**, 433001 (2017).
  - [10] S. Ghose, I. Robinson, P. Bennett, and F. Himpfel, *Surf. Sci.* **581**, 199 (2005).
  - [11] W. Voegeli, T. Takayama, T. Shirasawa, M. Abe, K. Kubo, T. Takahashi, K. Akimoto, and H. Sugiyama, *Phys. Rev. B* **82**, 075426 (2010).
  - [12] S. C. Erwin and F. J. Himpfel, *Nat. Commun.* **1**, 58 (2010).
  - [13] M. Krawiec, *Phys. Rev. B* **81**, 115436 (2010).
  - [14] J. N. Crain, A. Kirakosian, K. N. Altmann, C. Bromberger, S. C. Erwin, J. L. McChesney, J.-L. Lin, and F. J. Himpfel, *Phys. Rev. Lett.* **90**, 176805 (2003).
  - [15] J. N. Crain, J. L. McChesney, F. Zheng, M. C. Gallagher, P. C. Snijders, M. Bissen, C. Gundelach, S. C. Erwin, and F. J. Himpfel, *Phys. Rev. B* **69**, 125401 (2004).
  - [16] J. R. Ahn, P. G. Kang, K. D. Ryang, and H. W. Yeom, *Phys. Rev. Lett.* **95**, 196402 (2005).
  - [17] I. Song, D.-H. Oh, H.-C. Shin, S.-J. Ahn, Y. Moon, S.-H. Woo, H. J. Choi, C.-Y. Park, and J. R. Ahn, *Nano Lett.* **15**, 281 (2015).
  - [18] I. Barke, F. Zheng, T. K. Rügheimer, and F. J. Himpfel, *Phys. Rev. Lett.* **97**, 226405 (2006).
  - [19] J. Aulbach, J. Schäfer, S. C. Erwin, S. Meyer, C. Lohö, J. Settelein, and R. Claessen, *Phys. Rev. Lett.* **111**, 137203 (2013).
  - [20] F. Edler, I. Miccoli, H. Pfnür, and C. Tegenkamp, *Phys. Rev. B* **100**, 045419 (2019).
  - [21] T. Lichtenstein, Z. Mamiyev, C. Braun, S. Sanna, W. G. Schmidt, C. Tegenkamp, and H. Pfnür, *Phys. Rev. B* **97**, 165421 (2018).
  - [22] Z. Mamiyev, M. Tzschoppe, C. Huck, A. Pucci, and H. Pfnür, *J. Phys. Chem. C* **123**, 9400 (2019).



- [23] B. Hafke, T. Frigge, T. Witte, B. Krenzer, J. Aulbach, J. Schäfer, R. Claessen, S. C. Erwin, and M. Horn-von Hoegen, *Phys. Rev. B* **94**, 161403(R) (2016).
- [24] H. W. Yeom, S. W. Jung, J. S. Shin, J. Kim, K. S. Kim, K. Miyamoto, T. Okuda, H. Namatame, A. Kimura, and M. Taniguchi, *New J. Phys.* **16**, 093030 (2014).
- [25] M. Krawiec, M. Kopciuszynski, and R. Zdyb, *Appl. Surf. Sci.* **373**, 26 (2016), 7th International Workshop on Surface Physics: Molecular Nanostructures [IWSP-2015].
- [26] J. Aulbach, Doctoral thesis, Universität Würzburg (2018).
- [27] C. Braun, S. Neufeld, U. Gerstmann, S. Sanna, J. Plaickner, E. Speiser, N. Esser, and W. G. Schmidt, *Phys. Rev. Lett.* **124**, 146802 (2020).
- [28] Z. Mamiyev, C. Fink, K. Holtgrewe, H. Pfnür, and S. Sanna, *Phys. Rev. Lett.* **126**, 106101 (2021).
- [29] J. Plaickner, E. Speiser, C. Braun, W. G. Schmidt, N. Esser, and S. Sanna, *Phys. Rev. B* **103**, 115441 (2021).
- [30] A. V. Moroz and C. H. W. Barnes, *Phys. Rev. B* **60**, 14272 (1999).
- [31] A. Manchon, H. C. Koo, J. Nitta, S. M. Frolov, and R. A. Duine, *Nat. Mater.* **14**, 871 (2015).
- [32] A. Iucci, *Phys. Rev. B* **68**, 075107 (2003).
- [33] A. Schulz, A. De Martino, and R. Egger, *Phys. Rev. B* **82**, 033407 (2010).
- [34] A. Schulz, A. De Martino, P. Ingenhoven, and R. Egger, *Phys. Rev. B* **79**, 205432 (2009).
- [35] B. Braunecker, G. I. Japaridze, J. Klinovaja, and D. Loss, *Phys. Rev. B* **82**, 045127 (2010).
- [36] J. A. Riera, *Phys. Rev. B* **88**, 045102 (2013).
- [37] N. Kainaris and S. T. Carr, *Phys. Rev. B* **92**, 035139 (2015).
- [38] V. Gritsev, G. I. Japaridze, M. Pletyukhov, and D. Baeriswyl, *Phys. Rev. Lett.* **94**, 137207 (2005).
- [39] A. V. Moroz, K. V. Samokhin, and C. H. W. Barnes, *Phys. Rev. B* **62**, 16900 (2000).
- [40] C. J. Pedder, T. Meng, R. P. Tiwari, and T. L. Schmidt, *Phys. Rev. B* **94**, 245414 (2016).
- [41] A. N. Kocharian, G. W. Fernando, K. Fang, K. Palandage, and A. V. Balatsky, *AIP Adv.* **6**, 055711 (2016).
- [42] B. Hafke, C. Brand, T. Witte, B. Sothmann, M. Horn-von Hoegen, and S. C. Erwin, *Phys. Rev. Lett.* **124**, 016102 (2020).
- [43] Z. Mamiyev, S. Sanna, T. Lichtenstein, C. Tegenkamp, and H. Pfnür, *Phys. Rev. B* **98**, 245414 (2018).
- [44] P. Chudzinski, M. Gabay, and T. Giamarchi, *Phys. Rev. B* **78**, 075124 (2008).
- [45] A. O. Gogolin, A. A. Nersesyan, and A. M. Tsvelik, *Bosonization and Strongly Correlated Systems* (Cambridge University Press, Cambridge, UK, 2004).
- [46] D. Scalapino, *Physica C* **282-287**, 157 (1997), Materials and Mechanisms of Superconductivity High Temperature Superconductors V.
- [47] A. Nocera, Y. Wang, N. D. Patel, G. Alvarez, T. A. Maier, E. Dagotto, and S. Johnston, *Phys. Rev. B* **97**, 195156 (2018).
- [48] P. Chudzinski, *Phys. Rev. B* **103**, 155122 (2021).
- [49] F. H. L. Essler and A. M. Tsvelik, *Phys. Rev. Lett.* **90**, 126401 (2003).
- [50] J. Aulbach, S. C. Erwin, J. Kemmer, M. Bode, J. Schäfer, and R. Claessen, *Phys. Rev. B* **96**, 081406(R) (2017).
- [51] H. Zhang, J.-H. Choi, Y. Xu, X. Wang, X. Zhai, B. Wang, C. Zeng, J.-H. Cho, Z. Zhang, and J. G. Hou, *Phys. Rev. Lett.* **106**, 026801 (2011).
- [52] T.-H. Kim and H. W. Yeom, *Phys. Rev. Lett.* **109**, 246802 (2012).
- [53] S. T. Carr, A. O. Gogolin, and A. A. Nersesyan, *Phys. Rev. B* **76**, 245121 (2007).
- [54] L. Dudy, J. Aulbach, V. Rogalev, J. Schaefer, R. Claessen, and P. Chudzinski (unpublished).
- [55] E. L. Shirley, L. J. Terminello, A. Santoni, and F. J. Himpsel, *Phys. Rev. B* **51**, 13614 (1995).